Nanoscale

PAPER

View Article Online
View Journal | View Issue

Cite this: *Nanoscale*, 2022, **14**, 12437

Au_3-Decorated graphene as a sensing platform for O_2 adsorption and desorption kinetics†

Guillaume Libeert, [a] Ramasamy Murugesan, [b] Márton Guba,[c] Wout Keijers,[a] Simon Collienne, [d] Bart Raes,[a] Steven Brems,[e] Stefan De Gendt,[e,f] Alejandro V. Silhanek, [d] Tibor Höltzl, [c,g] Michel Houssa, [b,e] Joris Van de Vondel [a] and Ewald Janssens *[a]

Received 3rd June 2022,
Accepted 9th August 2022

DOI: 10.1039/d2nr03076d

rsc.li/nanoscale

The adsorption and desorption kinetics of molecules is of significant fundamental and applied interest. In this paper, we present a new method to quantify the energy barriers for the adsorption and desorption of gas molecules on few-atom clusters, by exploiting reaction induced changes of the doping level of a graphene substrate. The method is illustrated for oxygen adsorption on Au_3 clusters. The gold clusters were deposited on a graphene field effect transistor and exposed to O_2. From the change in graphene's electronic properties during adsorption, the energy barrier for the adsorption of O_2 on Au_3 is estimated to be 0.45 eV. Electric current pulses increase the temperature of the graphene strip in a controlled way and provide the required thermal energy for oxygen desorption. The oxygen binding energy on Au_3/graphene is found to be 1.03 eV and the activation entropy is 1.4 meV K^{-1}. The experimental values are compared and interpreted on the basis of density functional theory calculations of the adsorption barrier, the binding energy and the activation entropy. The large value of the activation entropy is explained by the hindering effect that the adsorbed O_2 has on the fluxional motion of the Au_3 cluster.

Introduction

The adsorption of oxygen molecules on metals has been a subject of intense experimental and computational research. This is due in part to the fact that it represents the first step in a wide range of industrially important chemical reactions, such as ethylene epoxidation or CO oxidation in heterogeneous catalysis, or the oxygen reduction reaction in electrocatalysis.[1] Upon adsorption of O_2 on metals, charge is transferred from the metal to the antibonding orbitals of the oxygen molecule. Depending on the amount of transferred charge, this results either in elongation or dissociation of the intramolecular bond and it activates the molecule for oxidative reactions. In order to get a complete picture of this process, both O_2 adsorption and desorption on metal surfaces have been studied experimentally. O_2 adsorption can be studied by the King–Wells technique to measure the sticking probability[2] and O_2 desorption can be studied by Temperature Programmed Desorption (TPD).[3] TPD can be used to determine the attempt frequency and activation energy for desorption.[4]

In the past years, O_2 activation on few-atom clusters has attracted considerable attention, because the electronic and geometric structure of these clusters are strongly size-dependent, allowing to tune their chemical reactivities.[5,6] Lei *et al.* used Ag_3 clusters as a catalyst for propylene epoxidation.[7] Corma *et al.* showed that the oxidation of thiophenol to disulfide can be catalyzed by Au_3 clusters.[8] Concepción *et al.* found a cluster-size-dependent reactivity between Cu clusters and oxygen.[9] Probably the most studied oxidation reaction on metal clusters is CO oxidation, which was shown to be catalyzed by Pt and Au clusters.[10–12]

Despite the clear importance of few-atom clusters as oxygenation catalysts, few studies have experimentally investigated the adsorption and desorption kinetics of molecular oxygen on clusters. Sangnier *et al.* used TPD to study the desorption

[a]*Quantum Solid-State Physics, Department of Physics and Astronomy, KU Leuven, Leuven, Belgium. E-mail: ewald.janssens@kuleuven.be*
[b]*Semiconductor Physics Laboratory, Department of Physics and Astronomy, KU Leuven, Leuven, Belgium*
[c]*Budapest University of Technology and Economics, Department of Inorganic and Analytical Chemistry and MTA-BME Computation driven research group, Budapest, Hungary*
[d]*Experimental Physics of Nanostructured Materials, Q-MAT, CESAM, Université de Liege, Sart Tilman, Belgium*
[e]*Imec, Leuven, Belgium*
[f]*Division of Molecular Design and Synthesis, Department of Chemistry, KU Leuven, Leuven, Belgium*
[g]*Furukawa Electric Institute of Technology Ltd., Budapest, Hungary*

† Electronic supplementary information (ESI) available: Details about the device fabrication, collision frequency calculation, computed geometries and band structures, relation between resistivity and V_{CNP}, power dissipation simulations, and entropy estimation from the molecular dynamics simulations. See DOI: https://doi.org/10.1039/d2nr03076d

of O_2 from Pt_{13} clusters, but the adsorption barrier was only assessed computationally.[13] Conversely, to the best of our knowledge, there is only one experimental study on the adsorption of O_2 on deposited few-atom clusters, namely the X-ray photoelectron spectroscopy study of Bower *et al.* on Si_n clusters (n = 10, 13 and 40–50).[14] Likely, this lack of experimental data is due to the low surface coverage of the deposited clusters that is typically needed to prevent sintering, thus resulting in low signals. Therefore, a sensitive technique which can measure the adsorption kinetics of O_2 on clusters is highly desirable.

Graphene has been investigated extensively for gas sensing applications because of its high sensitivity to adsorbed particles,[15] which can be further improved by functionalization,[16] introducing defects,[17] or by forming composites with polymers or metal oxides.[18–20] It has been shown that different adsorbed molecules have a different effect on the noise spectrum of graphene, allowing to use graphene as a selective sensor.[21] In addition, graphene offers the advantage of outstanding stability and thermal conductivity.[22] Due to its low heat capacity, the temperature of graphene can be increased significantly by relatively small currents, maximizing energy efficiency.[23–25] For example, Scheerder *et al.* deposited Au_3 clusters on graphene and used current-induced heating to induce coalescence of the deposited Au_3 clusters.[26]

In this work, we propose an innovative approach to study the adsorption and desorption kinetics of molecules adsorbed on clusters, making full use of graphene's unique sensing and thermal properties. In our original approach, graphene serves both as a sensor and a heating element. Specifically, clusters composed of three gold atoms were deposited on a Graphene Field Effect Transistor (GFET). This functionalizes the graphene strip as an oxygen detector, as was shown in a previous publication by some of the authors.[27] In the current article, we develop this idea further by controlled *in situ* measurements during the oxygen molecule adsorption and desorption processes that allow to quantify the adsorption barrier, the desorption energy as well as entropy changes during the desorption process, values that so far have been very challenging to obtain experimentally.

Methodology

The experimental procedure of depositing few-atom clusters on graphene devices was introduced in previous publications.[26,27] In brief, the electronic measurements were done on a GFET, which consists of a graphene layer deposited on top of a 300 nm SiO_2 layer thermally grown on a heavily doped silicon substrate. When a back-gate voltage V_g is applied to the silicon substrate, an electric field induces charge carriers in the graphene strip, changing its resistivity. Au_3 clusters were deposited on these GFETs by the cluster beam deposition (CBD) technique with controlled energy and density. Magnetron sputtering of a gold target by Ar^+ ions created a plasma that condensed into gold clusters through collisions with He carrier gas in a liquid nitrogen cooled condensation chamber. After expansion into vacuum, anionic clusters were guided towards a quadrupole mass spectrometer (QMS), which selects Au_3^- clusters with single atom precision. The size-selected clusters are deposited on the GFET with a kinetic energy distribution of (5 ± 3) eV per cluster or (1.7 ± 1.0) eV per atom, as measured by a beam probe with a variable stopping potential.[26] According to ref. 28, a kinetic energy of 15.6 eV per atom is needed for Au clusters to introduce defects in the graphene. We therefore can assume that the Au clusters are soft landed and do not introduce defects in the graphene. The deposited cluster density was quantified by integration of the electric current on the sample during deposition.

Subsequently, O_2 gas was introduced in the Ultra High Vacuum (UHV) cluster deposition chamber through a needle valve, causing a pressure rise from the base pressure of 3×10^{-9} mbar to 10^{-4} mbar. The electronic properties of the graphene strip were monitored while exposing the sample with the gold clusters to the O_2 gas. After O_2 exposure, the graphene strip was heated in a controlled way by sending current pulses. The electrical resistivity was measured between the current pulses to quantify the oxygen desorption.

Electronic measurements

An optical microscope image of the used GFET is provided in Fig. 1a. The GFET consists of a graphene flake with Au/Ti current and voltage contacts on a SiO_2/Si^{++} substrate (see ESI† for details about the lithographic fabrication of the GFET). By applying a back-gate voltage difference V_g between the graphene strip flake and the Si^{++} substrate, the graphene strip is doped with electrons or holes, effectively changing its resistivity. The sheet resistivity can be calculated as $\rho_s = (V_{\Delta x}/I_B)\cdot(W/L)$, with $V_{\Delta x}$ the measured voltage difference between the voltage contacts, I_B the applied bias current (1 μA), and W and L respectively the width (10 μm) and the length (21 μm) of the rectangular flake. The dependence of the sheet resistivity on the back-gate voltage V_g, called the field-effect characteristic $\rho_s(V_g)$, is shown by the blue curve in Fig. 1b for the virgin device. The sheet resistivity is maximal at the charge neutrality point V_{CNP}. As a preparatory step, the device was annealed with a large current of 3.1 mA (at even higher currents the field effect characteristic becomes unstable), which corresponds to a dissipated electric power of $P_E = V{\cdot}I \approx 28.2$ mW. During the annealing V_{CNP} moved to a lower value. After annealing for half an hour V_{CNP} no longer moved and the annealing was stopped (red curve in Fig. 1b). The clusters were deposited with a density of 10^{14} clusters per cm^2. The effect of Au_3 deposition on $\rho_s(V_g)$ is illustrated in Fig. 1b. Because the Au_3 clusters dope the graphene strip with electrons (n-doping), V_{CNP} further shifted to lower values.[26] Apart from the evolution in V_{CNP}, it should also be noted that the maximal sheet resistivity also changed as a result of the applied actions. Upon annealing and cluster deposition, the maximal sheet resistivity respectively decreased and increased. Since this maximal sheet resistivity is mainly a measure of the presence of charged impurities,[29,30] we can conclude that current annealing

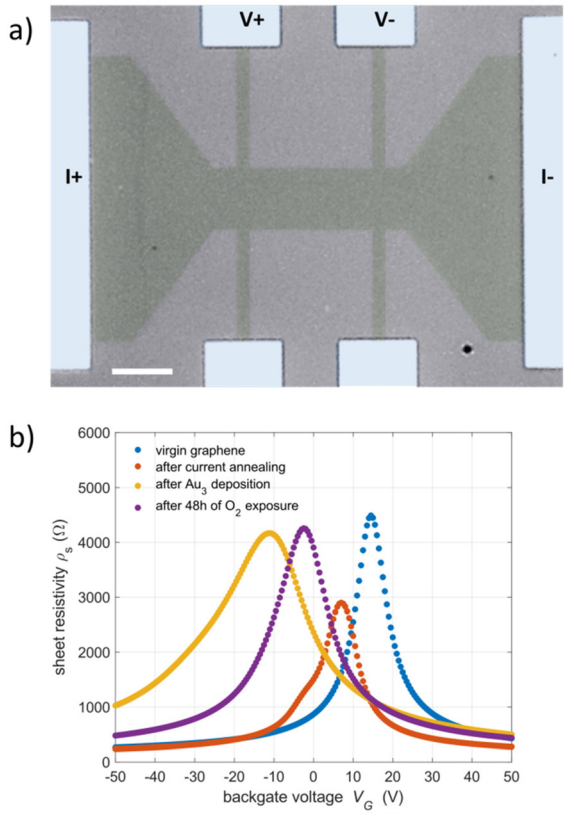

Fig. 1 (a) False-colored optical microscope image of a typical GFET. The white scalebar indicates 10 μm. The graphene strip is colored green. A bias current I_B is applied horizontally through the current contacts ($I+$ and $I-$). The voltage drop $V_{\Delta x}$ is measured over the voltage contacts ($V+$ and $V-$) in the longitudinal direction. By applying a back-gate voltage V_g the charge carrier density, and consequently the resistivity, of the graphene strip flake can be varied. (b) Comparison of the field-effect characteristic $\rho_s(V_g)$ of the pristine graphene device, the device after current annealing at 3.1 mA, after deposition of Au_3 with a density of 10^{14} clusters per cm^2 and after 48 hours of O_2 exposure.

reduced and cluster deposition increased the number of charged impurities. The decrease in charged impurities can be rationalized by the diffusion of resist residue upon annealing,[23] and the increase by the fact that Au_3 acts as a scattering center for charge carriers in graphene, thereby inducing impurity scattering and possibly phonon scattering.[26] Also, some of the charged clusters will land on insulating parts and will therefore not lose their charge upon deposition, effectively inducing mirror charges in the graphene strip, which can also serve as charged impurities that will increase the maximal resistivity. After the deposition, the evolution of the back-gate peak was monitored by sweeping the back-gate voltage periodically and by measuring the resultant change in sheet resistivity.

Sequential heating of the sample

After exposure of the sample to the oxygen gas, the desorption of O_2 molecules from the Au_3 clusters was induced by increasing the temperature of the graphene strip. The sample is initially at room temperature and heated by current pulses from 0.1 mA to 2.3 mA, increased in steps of 0.1 mA and sustained for a time Δt of 20 s. A pause of 1 s between each heating step allows the graphene strip to return to room temperature and to measure its resistivity. To relate the current to the power dissipation and the temperature of the graphene strip flake, a quantitative model developed by Bae *et al.* in ref. 24 was used. The obtained temperature profiles are non-uniform over the graphene strip due to the back-gate dependent resistivity. This non-uniformity is taken into account when calculating the oxygen desorption barriers. More details are provided in the ESI.†

Computational methodology

First-principles calculations in this work were performed with the VASP package that uses plane wave basis sets.[31–34] Projector-augmented wave (PAW) potentials describe the ion cores.[33] All the structures were relaxed using a 6 × 6 graphene supercell with an energy cut-off of 400 eV. The Brillouin zone was sampled on a 5 × 5 × 1 *k*-point mesh. A vacuum layer of 25 Å was used to avoid spurious interactions between the neighboring cells. The structures were relaxed until the forces between the atoms were lower than 25 meV $Å^{-1}$. The generalized gradient approximation (GGA) exchange and correlation functional of Perdew, Burke, and Ernzerhof (PBE) were employed.[35] To further account for the van der Waals (vdW) interactions, the DFT-D2 methods of Grimme have been incorporated in the calculations.[36] The parameters for the vdW functional were taken from Sławińska *et al.* with vdW radii of 1.772 Å, 1.452 Å & 1.342 Å and dispersion coefficients of 40.62 J nm^6 mol^{-1}, 1.75 J nm^6 mol^{-1} and 0.70 J nm^6 mol^{-1} for gold, carbon and oxygen atom, respectively.[37] The pair interaction radius was set to 12 Å. The global scaling factor and damping parameter were fixed to 0.75 and 20, respectively. The minimum energy pathway for the O_2 desorption reaction was obtained by performing nudged elastic band (NEB) simulations, with the spring constant value between the images set to −5.

Ab initio molecular dynamics simulations were carried out using the GPAW program,[38,39] in conjunction with the Atomic Simulation Environment.[40] We used the 6 × 4 orthogonal cell of graphene for the computations. The PBE functional and the D3 dispersion correction[41] together with the double-zeta polarized local Gaussian type basis set[42] were employed. The initial velocities were assigned to the nuclei according to the Maxwell–Boltzmann distribution at 300 K and the Nosé–Hoover thermostat was employed. 10 ps simulations were completed using a timestep of 1 fs. The entropies were estimated based on the Vibrational Density of States computed from the Velocity-Autocorrelation Function, as described in ref. 43. Further details are available in the ESI.†

Kinetics model

The adsorption or desorption of the O_2 molecules on the Au_3 cluster is quantified by changes in the graphene doping level.

Such change in doping results in a shift of the charge neutrality point V_{CNP}. Below, expressions are derived that allow to directly relate the shift of the V_{CNP} with the thermodynamic quantities of adsorption and desorption processes.

Doping of the graphene strip

It has been demonstrated that every deposited Au_3 cluster induces ε_e electrons (with $\varepsilon_e > 0$, n-doping) and every Au_3–O_2 complex ε_h electrons (with $\varepsilon_h < 0$, p-doping) in the graphene strip.[27] Consequently, ε_{tot} the total number of induced electrons in the graphene strip, equals $\varepsilon_e N_{Au_3} + \varepsilon_h N_{Au_3O_2}$, with N_{Au_3} the number of bare Au_3 clusters and $N_{Au_3O_2}$ the number of Au_3–O_2 complexes. Upon adsorption of one O_2 molecule on a Au_3 cluster, ε_{tot} changes by an amount $\varepsilon_h - \varepsilon_e = \varepsilon_{O_2}$. Therefore, the change in induced number of electrons $\Delta\varepsilon_{tot}$ during oxygen adsorption equals $\varepsilon_{O_2} N_a$, with N_a the number of oxygen adsorption events. It is assumed that every Au_3 cluster can accommodate only one oxygen molecule. DFT calculations have shown that the adsorption of two or more oxygen molecules on the Au_3 cluster is not stable at room temperature on the timescale of minutes. Pristine graphene devices (without gold clusters) were found not to respond to the O_2 gas at the used pressure of 10^{-4} mbar, which is consistent with calculated very small O_2 binding energies (order of 0.1 eV),[44] implying no stable oxygen binding on pristine graphene at room temperature.

Graphene doping results in a shift in charge neutrality point ΔV_{CNP}:[27]

$$\Delta\varepsilon_{tot} = -\alpha A \Delta V_{CNP} \tag{1}$$

with α the SiO_2 capacitance per unit area (7.2×10^{10} V^{-1} cm^{-2}), and A the area of the graphene strip between the voltage probes (210 μm^2). This equation can be used for either the oxygen adsorption process, when $\Delta\varepsilon_{tot}$ equals $\varepsilon_{O_2} N_a$, or for the desorption process when $\Delta\varepsilon_{tot}$ equals $-\varepsilon_{O_2} N_d$ with N_d the number of oxygen desorption events.

Reaction kinetics

If there is no sequential adsorption of molecular oxygen and no oxygen desorption takes place, the only relevant reaction during oxygen exposure is $Au_3/G + O_2 \rightarrow Au_3O_2/G$, which takes place at reaction rate $\nu_a = -dN_{Au_3}/dt$. For an adsorption reaction, where the reaction rate is constrained by the collision frequency between the gas and the adsorption site, the reaction rate can be approximated by collision theory:[45]

$$\nu_a = Z\rho \exp(-E_a/k_b T) \tag{2}$$

With Z the collision frequency, ρ a dimensionless steric factor and E_a the adsorption energy barrier. The collision frequency of the O_2 molecules with the Au_3 cluster is given by (see derivation in ESI†):

$$Z = \frac{3 \cdot N_{Au_3}}{n_{ML}} \frac{P}{2} \sqrt{\frac{\pi}{m k_b T}} \tag{3}$$

with P the pressure in the chamber (10^{-4} mbar), m the mass of an O_2 molecule, k_B the Boltzmann constant, T the temperature of the O_2 gas during exposure (293 K), N_{Au_3} the number of deposited clusters and n_{ML} the density of a Au monolayer (1.52×10^{15} atoms per cm^2).[46] The time evolution of N_{Au_3} and $N_{Au_3O_2}$ is then given by:

$$N_{Au_3}(t) = N_{Au_3,0} e^{-bt} \tag{4}$$

and

$$N_{Au_3O_2}(t) = N_{Au_3,0}(1 - e^{-bt}) \tag{5}$$

with constants $b = \frac{3P}{2n_{ML}} \sqrt{\frac{\pi}{m k_b T}} \rho \exp(-E_a/k_B T)$ and $N_{Au_3,0}$ the number of deposited Au_3 clusters.

Once the oxygen inlet is closed and the sample is heated, only oxygen desorption takes place. Assuming the desorption is a first order reaction $Au_3O_2/G \rightarrow Au_3/G + O_2$, the reaction rate is proportional to the amount of reactant:

$$\nu_d = k_d N_{Au_3O_2} \tag{6}$$

where the reaction rate constant k_d is given by the Eyring equation:[45]

$$k_d = \frac{k_B T}{h} e^{-\Delta G^{\ddagger}/k_b T} \tag{7}$$

with h the Planck constant and $\Delta G^{\ddagger} = \Delta H^{\ddagger} - T\Delta S^{\ddagger}$ the difference in Gibbs free energy between bound state and transition state. $\Delta H^{\ddagger}$ is the enthalpy of activation (which, since our experiments were done at constant pressure and volume, is equal to the energy of activation $\Delta E^{\ddagger}$) and $\Delta S^{\ddagger}$ the entropy of activation. For the temperature ranges that we are interested in (290–340 K), the attempt frequency $k_B T/h$ is in the order of 6×10^{12} s^{-1}, but the reaction rate, and hence the desorption kinetics, can be substantially increased by a large $\Delta S^{\ddagger}$. Under these conditions the number of Au_3O_2 complexes on graphene evolves as:

$$\begin{aligned} N_{Au_3O_2}(t) &= N_{Au_3O_2,i} e^{-k_d t} \\ &= N_{Au_3O_2,i} \exp\left(-\frac{k_B T}{h} \exp\left(\frac{\Delta S^{\ddagger}}{k_B}\right) \exp\left(-\frac{\Delta E^{\ddagger}}{k_B T}\right) t\right) \\ &= N_{Au_3O_2,i} D(t,T) \end{aligned} \tag{8}$$

where $N_{Au_3O_2,\,i}$ is the initial number of reactants before desorption. In other words, if the ensemble of reactants is kept at temperature T, the number of surviving complexes after time t equals the number of initial complexes times a factor, which we call the desorption factor $D(t, T)$. In the experiment, the sample is initially at room temperature and subsequently stepwise heated for time interval Δt at increasing temperatures T_1, T_2, T_3,... with a pause between each heating step. Since the sample is kept at room temperature for multiple hours between the O_2 exposure and the annealing routines, during which there is almost no desorption, we can safely assume no desorption takes place in the pause between heating steps. Each temperature T_n corresponds to a desorption factor $D_n(t, T_n)$. After n heating steps, the number of remaining complexes

will be $N_{Au_3O_2,n} = N_{Au_3O_2,i}D_1D_2...D_n$ and the number of desorbed molecules after each step is

$$N_{dn} = N_{Au_3O_2,i}(1 - D_1D_2...D_n) \quad (9)$$

To account for the non-uniform temperature of the graphene, the probed sample is numerically discretized in rectangles and, assuming a constant initial density, the initial number of O_2–Au_3 complexes is calculated per rectangle. For each annealing step and for each rectangle, the desorption factors are calculated and N_{dn} is obtained by summing the desorbed molecules of each rectangle. One must then start with trial values for $\Delta E^{\ddagger}$ and $\Delta S^{\ddagger}$, calculate the desorption factors, and iteratively obtain the values for N_{dn}.

Results and discussion

Adsorption kinetics

The adsorption of O_2 molecules on Au_3 clusters results in a switch from n-doping of the graphene strip by the Au_3 clusters to p-doping by the Au_3–O_2 complexes.[27] This is reflected in a shift of the charge neutrality point to higher values during O_2 exposure, as shown by the graph in Fig. 1. In Fig. 2, the shift in charge neutrality point during the adsorption reaction $\Delta_a V_{CNP}$ is given as a function of time. Combining eqn (1) and (5), $\Delta_a V_{CNP}$ is given by:

$$\Delta_a V_{CNP} = \Delta_{a,max} V_{CNP}(1 - e^{-bt}) \quad (10)$$

with $\Delta_{a,max}V_{CNP}$ the theoretical maximum shift in V_{CNP} caused by oxygen adsorption, *i.e.* the shift of the charge neutrality point if all Au_3 clusters adsorb one oxygen molecule. The fitted parameters for the oxygen exposure data shown in Fig. 2 are $\Delta_{a,max}V_{CNP} = (3.9 \pm 0.1)$ V and $b = (6.1 \pm 0.1) \times 10^{-6}$ s^{-1}.

With this value for parameter b, it can be calculated that $\rho \exp(-E_a/k_BT)$ equals $(5.11 \pm 0.08) \times 10^{-8}$. While the values for ρ and $\exp(-E_a/k_BT)$ can not be separated, it is possible to make some estimates for E_a by considering a broad realistic range for ρ. If ρ is equal to unity, any collision between a Au_3 cluster and an oxygen molecule with enough kinetic energy to overcome the adsorption barrier would result in a bound state. If ρ is smaller than unity, the oxygen molecule and the Au_3 cluster need to have a specific orientation towards each other before the collision can result in a bound state.

Given the symmetry of the oxygen molecule and the Au_3 cluster, there are multiple collision configurations that will result in a bound state. Therefore, it is reasonable to assume that ρ will be close to unity. For a realistic ρ range from 1 to 0.1, one gets $E_a = (0.45 \pm 0.03)$ eV as experimental value for the energy barrier for the adsorption of an oxygen molecule on an Au_3 cluster. The error range on E_a is a consequence of the uncertainty on ρ and does not take into account other effects. The obtained value for $\Delta_{a,max}V_{CNP}$ can be used to obtain an experimental number of induced electrons ε_{tot} when every cluster is occupied by an oxygen molecule by using formula (1). By dividing with $N_{Au_3,0}$, based on the integration of current on the sample during deposition, one obtains a change in doping upon adsorption of a O_2 molecule $\varepsilon_{O_2} = (-0.0028 \pm 0.0001)$ e.

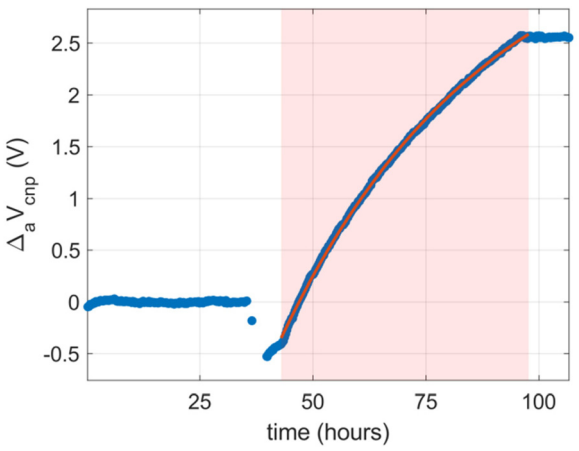

Fig. 2 The evolution of V_{CNP} during oxygen exposure. The time interval of oxygen exposure (from 43 h to 98 h) is highlighted by the pink shaded area. The red line is a fit of the data to eqn (10). The dip below the baseline before oxygen exposure is caused by a background measurement (see section 'Desorption kinetics').

Desorption kinetics

As discussed before, the oxygen could be desorbed by heating the graphene strip with current pulses. Large current pulses imply large source–drain biases which change the effective potential applied across the silica, and hence the effective back-gate voltage (see ESI† for more details). For this reason, the resistivity of the graphene strip was measured in between the current pulses. However, even in this case there is a background caused by hysteresis in the resistivity back-gate voltage relation.[47] To take this into account, the annealing measurement was also done before oxygen exposure and this measurement is used as a reference to eliminate the hysteresis.

A single annealing routine is performed as follows: first, the back-gate voltage is set to a value that corresponds to the point of highest derivative of the sheet resistivity peak, *i.e.* the point where $d\rho/dV_g$ is maximal. Then, an annealing current is sent through the sample. The current is increased stepwise from 0.1 to 2.3 mA in steps of 0.1 mA, each step lasting 20 s and with a pause to let the sample cool down to room temperature between the steps. After each step, the sheet resistivity was measured with a bias current of 1 μA. This annealing cycle is repeated twenty times. As explained in the ESI,† the values for the measured changes in the sheet resistivity can be converted to a shift in V_{CNP}. In Fig. 3a, the shifts in V_{CNP} obtained for the first annealing cycle done before and after the oxygen exposure are shown. As can be seen, V_{CNP} also shifts with the annealing current before oxygen exposure. This is caused by the above-mentioned hysteretic effect (and not by heating of the graphene strip since it cools down to room temperature in between current pulses). To disentangle this effect from the shift in V_{CNP} caused by the desorption of O_2 molecules, we subtract the ΔV_{CNP} values after O_2 exposure ($\Delta_O V_{CNP}$) from the

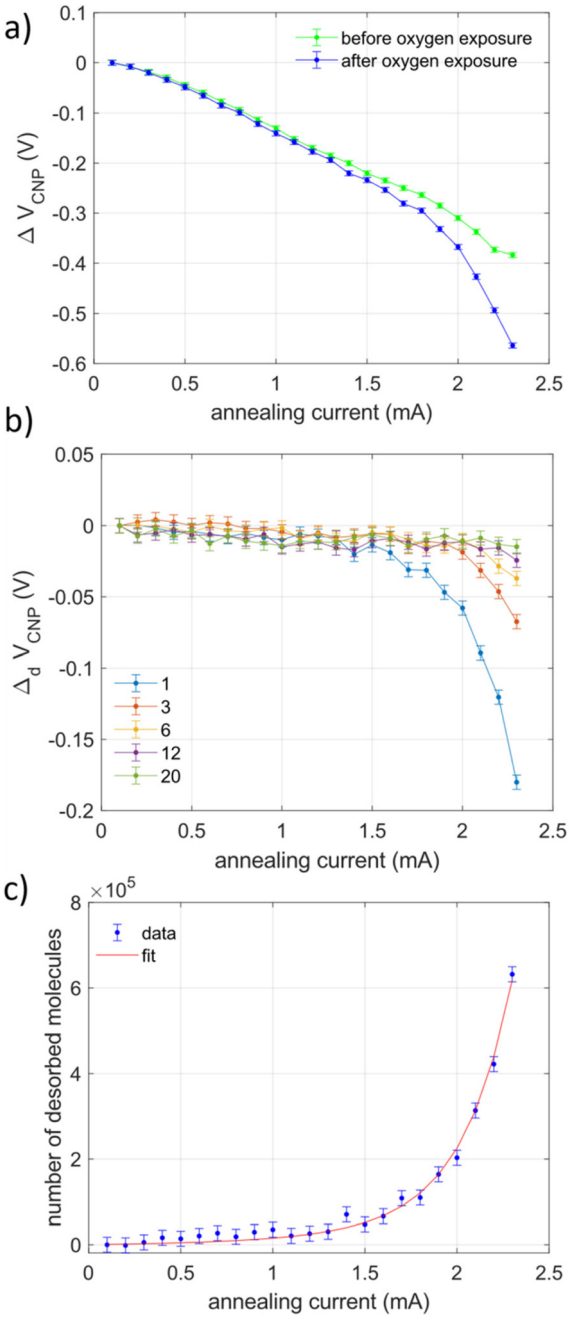

Fig. 3 (a) Shift in charge neutrality point as a function of the annealing current, before and after oxygen exposure. The first point of each measurement was used as reference. (b) Shift in charge neutrality point after consecutive 20 s annealing cycles, corrected for the effect of charging. The numbers in the legend are the index numbers of the annealing cycles. (c) Number of desorbed particles after each current pulse during the first annealing cycle. The statistical error bars represent the reproducibility of the measurements (on the same GFET). Systematic model uncertainty related to the use of eqn (1) is not included in panel (c).

ΔV_{CNP} values before O_2 exposure ($\Delta_{BO}V_{CNP}$) to obtain the shift in charge neutrality point caused by the O_2 desorption ($\Delta_d V_{CNP} = \Delta_O V_{CNP} - \Delta_{BO} V_{CNP}$). The results of this procedure for a selection of annealing cycles are shown in Fig. 3b. From these figures, it can be seen that $\Delta_d V_{CNP}$ is nearly zero after small annealing currents are applied (typically below 0.5 mA). Only after annealing the sample with larger currents, there is a negative $\Delta_d V_{CNP}$. The shift in charge neutrality point is caused by desorption of the O_2 molecules, which sets in at larger annealing currents and hence higher graphene temperatures. The twentyfold repetition was done to confirm that oxygen desorption disappears after repeated annealing cycles (see Fig. 3b). The shift in V_{CNP} can be converted to a number of desorbed molecules *via* eqn (1). A fit of the number of desorbed molecules with eqn (9), shown in Fig. 3c, provides $\Delta E^{\ddagger} = 1.48 \pm 0.08$ eV and $\Delta S^{\ddagger} = 1.4 \pm 0.3$ meV K^{-1}. The error bars take into account the correlation between these two values, as discussed in the ESI.†

Comparison of the experimental results with simulations

The energy barrier for the desorption of the oxygen molecule from the Au_3/graphene system is computed by the nudged elastic band method (NEB). The relaxed geometry obtained for the adsorbed and desorbed state of Au_3O_2/graphene system were used for the initial and final state of the reaction, as shown in Fig. 4. The intermediate state geometry is constructed from the interpolated images of the initial and final states. The NEB method optimizes the intermediate image along the reaction pathway to obtain the energy barrier during the reaction. The minimum energy pathway obtained for the desorption of the O_2 molecule from the Au_3/graphene surface is shown in Fig. 4. As can be seen from this figure, this is an activated process, which is also reflected in the O_2 bond length. In the desorbed state, the O–O bond length is 1.23 Å, in the transition state it elongates to 1.27 Å, and in the bound state it is 1.30 Å, indicating partial charge transfer to the O_2 molecule during adsorption. The energy of the transition state is 1.34 eV above the adsorbed state. The binding energy, obtained as the difference in energy, between adsorbed and

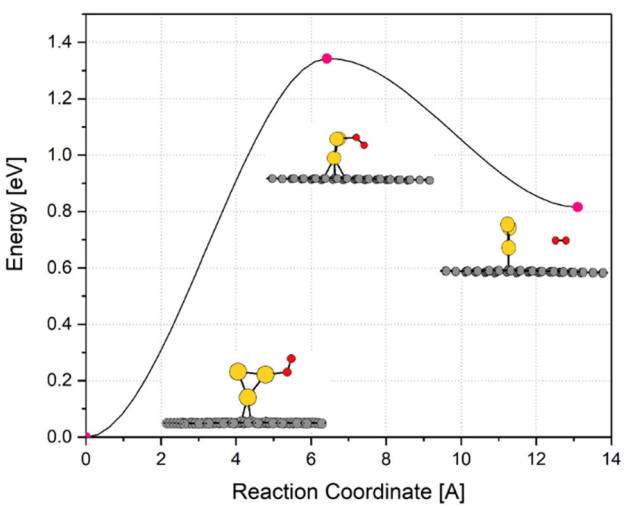

Fig. 4 The minimum energy pathway for the desorption of oxygen molecule on Au_3/graphene.

Table 1 Comparison of the experimentally and theoretically predicted values for the energy barrier, binding energy and activation entropy of the transition state

	Energy barrier (eV)	Binding energy (eV)	ε_{O_2} (e)	Activation entropy (meV K^{-1})
Exp.	0.45 ± 0.03	1.03 ± 0.08	−0.0028 ± 0.0001	1.4 ± 0.3
Theory	0.52	0.82	−0.0431	See text

desorbed state, is 0.815 eV. Therefore the computed energy barrier for the reaction O_2 + Au_3/graphene → O_2/Au_3/graphene is 1.34–0.815 = 0.52 eV. In Table 1, a comparison is made between the parameters extracted from theory and experiment. A number of observations can be made from this comparison.

Firstly, the general energy profile predicted by theory, *i.e.* a large adsorption barrier followed by a bound state with a binding energy of approximately 1 eV, is reproduced. The large binding energy and the elongation of the O_2 bond both point to chemisorption.[1]

Secondly, it should be noted that the experimental value for ε_{O_2} is an order of magnitude lower than the computational value for ε_{O_2}. This can be partly attributed to the fact that the calculation of the experimental value relies on the assumption that the number of clusters is exactly equal to the number calculated based on the neutralization current measured during deposition. This could be an overestimation, because a part of the clusters may coalesce to bigger structures. In a previous publication it was found that about 30% of the deposited Au_3 clusters undergo coalescence to larger nanoparticles, which do not dope the graphene.[26] Also, clusters that land on resist residue will also induce a neutralization current, but are not in direct contact with the graphene and will therefore not interact chemically with it. This possible overestimation of $N_{Au_3,0}$ significantly affects the experimental ε_{O_2} value but has little influence on the obtained thermodynamic quantities. The experimentally derived value of the adsorption barrier E_a only depends on the fitted time constant b, which is not a function of ε_{O_2}. In the desorption experiment, the number of desorbed O_2 molecules is calculated based on the same experimental ε_{O_2} value, so the numbers of deposited Au_3 clusters and desorbed O_2 molecules could be overestimated by the same factor. Therefore, the obtained values for $\Delta S^{\ddagger}$ and $\Delta E^{\ddagger}$ will not be affected significantly by a possible underestimation of ε_{O_2}.

Thirdly, the experimentally found difference in entropy between the bound state and the transition state $\Delta S^{\ddagger}$ of 1.4 ± 0.3 meV K^{-1} is not in agreement with the difference in vibrational entropies between the bound state and the transition state that is calculated by use of the harmonic oscillator approximation (only −0.033 meV K^{-1}) and, more in general is surprisingly large compared to the values typically calculated for molecules adsorbed on few-atom clusters by use of the harmonic oscillator approximation.[48] However, it should be noted that transition states are saddle points on the potential energy surface, so the harmonic oscillator approximation, which treats all adsorbates as harmonic oscillators and assumes that all entropy comes from the vibrational modes of these oscillators, is inaccurate. The large experimental $\Delta S^{\ddagger}$ value is reminiscent of the large $\Delta S^{\ddagger}$ value which was recently predicted for oxygen splitting on Au_8 and Au_{13} around 340 K.[49] In this case, the large $\Delta S^{\ddagger}$ was caused by melting of the transition state at a temperature where the initial state remained solid, causing a large entropy difference. More general, there has been a lot of interest lately in the effects of collective motions in few-atom clusters on the entropy of transition states, and its accelerating effects on reaction kinetics.[43]

Our experimental results illustrate that a good estimate of $\Delta S^{\ddagger}$ is critical for an accurate prediction of reaction rates. We further investigated the possible origin of the observed large entropy change during the oxygen dissociation using *ab initio* molecular dynamics simulations of the Au_3/G system with and without O_2. The gold–gold bond lengths and the cluster shape in a few snapshots of the simulations are depicted in Fig. 5. Both simulations start with the lowest energy, triangular cluster shape. Similarly to the recently studied Au_2–graphene system,[50] the clusters migrate easily on the graphene surface, which shows the importance of the (hindered) translation in both the bare and the oxygen bound Au_3/G systems. However, in reality, the translation of the clusters likely is hindered by imperfections not included in the our DFT calculations, such as resist residue or corrugations in the graphene sheet, which are inevitably present on every SiO_2 supported graphene device processed by lithographic methods.[51] Indeed, it was shown recently that the diffusion of few-atom clusters on a graphene sheet is suppressed by polymer chains that can act as trapping sites.[52,53] Thus, the effect of the hindered translation is approximately cancelled during the oxygen desorption and is expected to have a small contribution to the experimentally derived entropy change. However, the presence of the oxygen molecule considerably changes the dynamical behavior of the system. Because the bare Au_3 cluster on the graphene is highly flexible, the triangular cluster shape opens and closes several times on the time scale of the simulation, as is seen in the fast variations of the bond length plot (Fig. 5a), and also by the average gold–gold distances and their standard deviations (see the ESI† for the details). On the other hand, opening and closing is a much less frequent event in the case of the oxygen bound cluster. Nevertheless, the oxygen molecule is mobile and several quasi-dissociation events occur as well as a complete dissociation at about 9 ps simulation time. This timescale for desorption is shorter than the one observed in the experiment, but it should be noted that the DFT calculations predict a slightly weaker bond between the Au_3 cluster and the O_2 molecule than the one found experimentally and that reaction rates vary strongly with small changes in binding energy. Due to the low mass of the oxygen molecule, its motion has a small contribution to the entropy. Thus, the large entropy change is due to the oxygen molecule induced decrease of the flexibility of the cluster. These observations highlight the role of dynamical effects in the entropy. While the accurate determination of the entropy during the reaction[49] is beyond the Rigid Rotor Harmonic Oscillator approxi-

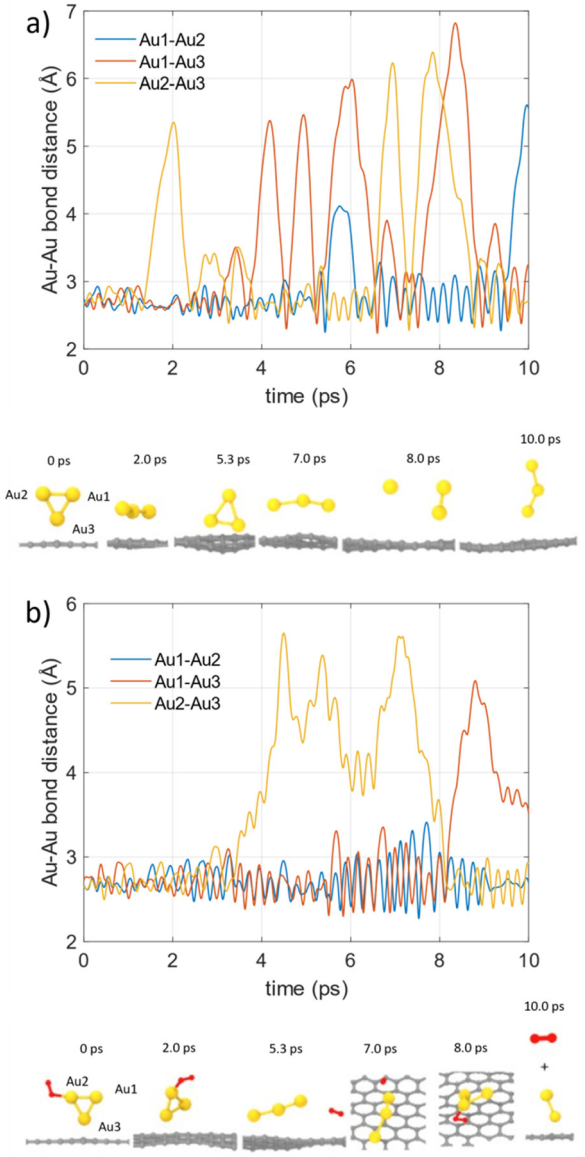

Fig. 5 Time evolution of the gold–gold bond lengths and the cluster shape in a few snapshots as obtained from the molecular dynamics simulations at 300 K (a) without oxygen (b) with oxygen.

mation and also beyond the scope of our paper, we estimated the entropy change from the above molecular dynamics computations (see the ESI† for the details). The estimated entropy change during the oxygen dissociation is 4.3 meV K^{-1} if we assume complete dissociation of the oxygen molecule (*i.e.* free translation in the gas phase), and 2.3 meV K^{-1} if we assume physisorption. While it must be emphasized that these values are rough estimations of the dissociation entropy, and thus cannot be directly compared to the experimentally derived activation entropy, their order of magnitude agrees and clearly show the importance of the cluster dynamics in the oxygen dissociation. This agreement could not be explained in the framework of the harmonic approximation.

Conclusions

It was shown that at room temperature and at an oxygen pressure of 10^{-4} mbar, oxygen molecules spontaneously adsorb on Au_3 clusters deposited on graphene, but the adsorption kinetics is slowed down by a significant energy barrier. Upon increasing the temperature by current annealing of the graphene strip, the desorption of the oxygen molecules can be activated. From this experiment, the difference in energy and entropy of the transition state upon desorption with respect to the bound state, can be inferred. By subtracting the energy barrier of the energy of the transition state, the binding energy (*i.e.* the difference in energy between the bound and the unbound state) can be obtained. Theory and experiment point to an activated process, with a significant energy barrier. The experimentally obtained entropy difference between the bound state and the transition state is surprisingly large, indicating that the cluster and the adsorbate are more fluxional than described by a harmonic oscillator approximation. Instead, molecular dynamics simulations were necessary to explain the observed activation entropy.

The method introduced here is an original approach that provides access to thermodynamic quantities related to the binding of molecules on nanostructured surfaces that are challenging to measure. The method can be applied to other systems and is expected to lead to new insights in the sorption kinetics of molecules on few-atom clusters.

Author contributions

J.V.d.V. and E.J. initiated the research on size-selected clusters with graphene. S.B. and S.D.G. did the CVD growth and transfer of graphene. G.L. and B.R. performed the experiments. G.L performed the data analysis. W.K. contributed to the cluster deposition. R.M. and M.H. performed the DFT calculations, NEB calculation and band structure calculation. T.H. and M.G. performed the molecular dynamics simulations and the entropy calculation. S.C., A.V.S. and G.L. contributed to the temperature model of current annealing in a GFET. G.L., J.V.d.V. and E.J. prepared the first version of the manuscript. All authors contributed to the data interpretation and participated in writing the manuscript.

Conflicts of interest

There are no conflicts to declare.

Acknowledgements

This research has been supported by the Research Foundation-Flanders (FWO project G.0D56.19N), by the KU Leuven–Budapest University of Technology and Economics joint research funding (CELSA/18/032) and by the European Union's Horizon 2020 Research and Innovation Programme under

grant agreement 881603. Part of the computational resources and services used in this work have been provided by the VSC (Flemish Supercomputer Center), funded by the Research Foundations-Flanders (FWO) and the Flemish Government – Department EWI. T. H. thanks the Hungarian Academy of Sciences for the János Bolyai research scholarship (BO/00642/21/7). The work of A. V. S. has been financially supported by the FWO and F.R.S.-FNRS under the Excellence of Science (EOS) project O.0028.22.

References

1 M. M. Montemore, M. A. van Spronsen, R. J. Madix and C. M. Friend, *Chem. Rev.*, 2017, **118**, 2816–2862.
2 W. A. Brown, R. Kose and D. A. King, *Chem. Rev.*, 1998, **98**, 797–832.
3 V. Rakić and L. Damjanović, Temperature-programmed desorption (TPD) methods, in *Calorimetry and thermal methods in catalysis*, ed. A. Auroux, Springer, Berlin, Heidelberg, first edition, 2013, pp. 131–174.
4 C. T. Campbell and J. R. Sellers, *J. Am. Chem. Soc.*, 2012, **134**, 18109–18115.
5 Z. Luo, A. W. Castleman Jr. and S. N. Khanna, *Chem. Rev.*, 2016, **116**, 14456–14492.
6 A. C. Reber and S. N. Khanna, *Acc. Chem. Res.*, 2017, **50**, 255–263.
7 Y. Lei, F. Mehmood, S. Lee, J. Greeley, B. Lee, S. Seifert, *et al.*, *Science*, 2010, **328**, 224–228.
8 A. Corma, P. Concepción, M. Boronat, M. J. Sabater, J. Navas, M. J. Yacaman, *et al.*, *Nat. Chem.*, 2013, **5**, 775–781.
9 P. Concepción, M. Boronat, S. García-García, E. Fernández and A. Corma, *ACS Catal.*, 2017, **7**, 3560–3568.
10 C. Yin, F. R. Negreiros, G. Barcaro, A. Beniya, L. Sementa, E. C. Tyo, *et al.*, *J. Mater. Chem. A*, 2017, **5**, 4923–4931.
11 A. Beniya, S. Higashi, N. Ohba, R. Jinnouchi, H. Hirata and Y. Watanabe, *Nat. Commun.*, 2020, **11**, 1–10.
12 S. Lee, C. Fan, T. Wu and S. L. Anderson, *J. Am. Chem. Soc.*, 2004, **126**, 5682–5683.
13 A. Sangnier, M. Matrat, A. Nicolle, C. Dujardin and C. Chizallet, *J. Phys. Chem. C*, 2018, **122**, 26974–26986.
14 J. E. Bower and M. F. Jarrold, *J. Chem. Phys.*, 1992, **97**(11), 8312–8321.
15 F. Schedin, A. K. Geim, S. V. Morozov, E. W. Hill, P. Blake, M. I. Katsnelson, *et al.*, *Nat. Mater.*, 2007, **6**, 652–655.
16 S. Baachaoui, S. Aldulaijan, L. Sementa, A. Fortunelli, A. Dhouib and N. Raouafi, *J. Phys. Chem. C*, 2021, **125**, 26418–26428.
17 F. Ricciardella, S. Vollebregt, T. Polichetti, M. Miscuglio, B. Alfano, M. L. Miglietta, *et al.*, *Nanoscale*, 2017, **9**, 6085–6093.
18 G. R. Berdiyorov, H. Abdullah, M. Al Ezzi, G. V. Rakhmatullaeva, H. Bahlouli and N. Tit, *AIP Adv.*, 2016, **6**, 125102.
19 D. Cortés-Arriagada, N. Villegas-Escobar and D. E. Ortega, *Appl. Surf. Sci.*, 2018, **427**, 227–236.
20 W. Tian, X. Liu and W. Yu, *Appl. Sci.*, 2018, **8**, 1118.
21 S. Rumyantsev, G. Liu, M. S. Shur, R. A. Potyrailo and A. A. Balandin, *Nano Lett.*, 2012, **12**, 2294–2298.
22 J. H. Seol, I. Jo, A. L. Moore, L. Lindsay, Z. H. Aitken, M. T. Pettes, *et al.*, *Science*, 2010, **328**, 213–216.
23 J. Moser, A. Barreiro and A. Bachtold, *Appl. Phys. Lett.*, 2007, **91**, 163513.
24 M. H. Bae, Z. Y. Ong, D. Estrada and E. Pop, *Nano Lett.*, 2010, **10**, 4787–4793.
25 M. Freitag, H. Y. Chiu, M. Steiner, V. Perebeinos and P. Avouris, *Nat. Nanotechnol.*, 2010, **5**, 497–501.
26 J. E. Scheerder, T. Picot, N. Reckinger, T. Sneyder, V. S. Zharinov, J. F. Colomer, *et al.*, *Nanoscale*, 2017, **9**, 10494–10501.
27 J. E. Scheerder, S. Liu, V. S. Zharinov, N. Reckinger, J. F. Colomer, H. P. Cheng, *et al.*, *Adv. Mater. Interfaces*, 2018, **5**, 1801274.
28 M. Di Vece, S. Palomba and R. E. Palmer, *Phys. Rev. B: Condens. Matter Mater. Phys.*, 2005, **72**, 073407.
29 S. Adam, E. H. Hwang, V. M. Galitski and S. D. Sarma, *Proc. Natl. Acad. Sci. U. S. A.*, 2007, **104**, 18392–18397.
30 V. E. Dorgan, M. H. Bae and E. Pop, *Appl. Phys. Lett.*, 2010, **97**, 082112.
31 G. Kresse and J. Hafner, *Phys. Rev. B: Condens. Matter Mater. Phys.*, 1993, **47**, 558.
32 G. Kresse and J. Furthmüller, *Comput. Mater. Sci.*, 1996, **6**, 15–50.
33 G. Kresse and D. Joubert, *Phys. Rev. B: Condens. Matter Mater. Phys.*, 1999, **59**, 1758.
34 P. E. Blöchl, *Phys. Rev. B: Condens. Matter Mater. Phys.*, 1994, **50**, 17953.
35 J. P. Perdew, K. Burke and M. Ernzerhof, *Phys. Rev. Lett.*, 1996, **77**, 3865.
36 S. Grimme, *J. Comput. Chem.*, 2006, **27**, 1787–1799.
37 J. Sławińska, P. Dabrowski and I. Zasada, *Phys. Rev. B: Condens. Matter Mater. Phys.*, 2011, **83**, 245429.
38 J. J. Mortensen, L. B. Hansen and K. W. Jacobsen, *Phys. Rev. B: Condens. Matter Mater. Phys.*, 2005, **71**, 035109.
39 J. Enkovaara, C. Rostgaard, J. J. Mortensen, J. Chen, M. Dułak, L. Ferrighi, *et al.*, *J. Phys.: Condens. Matter*, 2010, **22**, 253202.
40 A. H. Larsen, J. J. Mortensen, J. Blomqvist, I. E. Castelli, R. Christensen, M. Dułak, *et al.*, *J. Phys.: Condens. Matter*, 2017, **29**, 273002.
41 S. Grimme, J. Antony, S. Ehrlich and H. Krieg, *J. Chem. Phys.*, 2010, **132**, 154104.
42 A. H. Larsen, M. Vanin, J. J. Mortensen, K. S. Thygesen and K. W. Jacobsen, *Phys. Rev. B: Condens. Matter Mater. Phys.*, 2009, **80**, 195112.
43 G. Collinge, S. F. Yuk, M. T. Nguyen, M. S. Lee, V. A. Glezakou and R. Rousseau, *ACS Catal.*, 2020, **10**, 9236–9260.
44 F. Mehmood, R. Pachter, W. Lu and J. J. Boeckl, *J. Phys. Chem. C*, 2013, **117**, 10366–10374.

45 S. K. Upadhyay, *Chemical kinetics and reaction dynamics*, Springer, Dordrecht, 2007.
46 L. M. Yang, M. Dornfeld, T. Frauenheim and E. Ganz, *Phys. Chem. Chem. Phys.*, 2015, **17**, 26036–26042.
47 H. Wang, Y. Wu, C. Cong, J. Shang and T. Yu, *ACS Nano*, 2010, **4**, 7221–7228.
48 M. Jia, J. Vanbuel, P. Ferrari, W. Schöllkopf, A. Fielicke, M. T. Nguyen, *et al.*, *J. Phys. Chem. C*, 2020, **124**, 7624–7633.
49 J. J. Sun and J. Cheng, *Nat. Commun.*, 2019, **10**, 1–7.
50 M. Zarshenas, V. Gervilla, D. G. Sangiovanni and K. Sarakinos, *Phys. Chem. Chem. Phys.*, 2021, **23**, 13087–13094.
51 M. Ishigami, J. H. Chen, W. G. Cullen, M. S. Fuhrer and E. D. Williams, *Nano Lett.*, 2007, **7**, 1643–1648.
52 I. Lado-Touriño and A. Páez-Pavón, *Nanomaterials*, 2021, **11**, 1378.
53 S. R. Plant, L. Cao, F. Yin, Z. W. Wang and R. E. Palmer, *Nanoscale*, 2014, **6**, 1258–1263.